

RADIA Simulation of the CLS Storage Ring Quadrupole

5.2.31.3

Date: 1999-07-21

Copyright 2000, Canadian Light Source Inc. This document is the property of Canadian Light Source Inc. (CLS). No exploitation or transfer of any information contained herein is permitted in the absence of an agreement with CLS, and neither the document nor any such information may be released without the written consent of CLS.

Canadian Light Source
107 North Road
University of Saskatchewan
Saskatoon, Saskatchewan Canada

Signature

Date

Original on File – Signed by

Author	_____	_____
	R.E. Pywell	
Reviewer #1	_____	_____
	L.O. Dallin	
Reviewer #2	_____	_____
	J.C. Bergstrom	
Approver	_____	_____
	M.S. de Jong	

REVISION HISTORY

<i>Revision</i>	<i>Date</i>	<i>Description</i>	<i>Author</i>
0	1999-07-21	Issued for use.	R.E. Pywell



Saskatchewan Accelerator Laboratory
University of Saskatchewan
Saskatoon SK S7N 5C6 Canada

subject: **RADIA Simulation of the CLS Storage Ring Quadrupole**

date: **July 21, 1999**

from: **Rob Pywell**

reference: 2.1.30

ABSTRACT

The simulation of the CLS Storage Ring Quadrupole, Q3, using the 3D code RADIA is presented. The limitations of this code for detailed analysis of multipole components is discussed. The quadrupole field strengths were found to be about 4% lower than that predicted by the 2D code POISSON. The effective length of the quadrupole is investigated for various chamfer angles on the pole tip ends. It is concluded that a chamfer angle of 20° is required for the effective length of the quadrupole to be 277 mm.

1. The RADIA code

RADIA is a fast multi-platform software package dedicated to 3D magnetostatics computation. It is optimized for the design of undulators and wigglers made with permanent magnets, coils and linear/nonlinear soft magnetic materials. RADIA has been heavily benchmarked with a commercially available finite element package and with real devices built at the ESRF Insertion Devices Laboratory. Complete details of the operation of RADIA are available on the WEB at <http://www.esrf.fr/machine/support/ids/Public/Codes/software.html>.

The code runs as an add-on application to Mathematica which handles the manipulation of the objects specifying the elements in the problem. Mathematica code can then be used to analysis the results from the RADIA calculations, e.g. to calculate multipole components.

The method used in RADIA belongs to the category of boundary Integral Methods and differs strongly from the Finite Element Methods (FEM). Volume objects are created, and material properties are applied to these objects. Each object can be subdivided into a number of smaller objects for which one tries to solve for the general problem in terms of the magnetization. The solution is performed by building a large matrix in memory which represents the mutual interactions between the objects. This is called the Interaction Matrix. The final magnetization in each small object is obtained iteratively, by a sequence of multiplications of the Interaction Matrix by an instant magnetization vector, taking into account the material properties. This is called the Relaxation procedure. In this approach, one applies some kind of segmentation to the field-producing objects

(typically iron) but, contrary to the FEM approach, one does not need to mesh the vacuum. The relaxation procedure continues until the average stability, from one iteration to the next, of the magnetization in the problem is less than a specified value. In this analysis I have chosen this parameter to be 1×10^{-5} T. This does not represent the accuracy of the field results however. That depends on the segmentation of the problem. i.e. the number of small objects into which each object is split.

One “problem” with RADIA is that there is no clear way to determine ahead of time the degree of segmentation of each element needed to provide the required accuracy in the results. This can only be determined by changing the segmentation of each element and seeing how sensitive the results are to these changes; then increasing the segmentation until the results converge. Unfortunately it is possible to hit on combinations of segmentation values where the problem does not converge within a reasonable number of iterations. It is possible that changing the segmentation of one element, in one dimension, by a small amount (e.g. changing the number of slices from 4 to 5), changes the problem from one that converges rapidly to one that is divergent. If the problem does converge, however, the answers are correct to within the accuracy possible with that number of segments.

For this problem I have found that, with the maximum degree of segmentation possible with this computer, field values calculated are only stable to within about 1% (as discussed in section 5). Thus extraction of multipole components, effective lengths etc. can only be determined to approximately this order of accuracy. Thus it is not possible to check if we have remnant field errors less than 0.001 (0.1%) for comparison with the poisson calculation of Dallin (2.1.8G).

The limitations for increasing the accuracy of the calculation, by increasing the degree of segmentation, are time and computer memory. When the interaction matrix reaches the computer memory size the paging activity becomes so large that computation times increase dramatically. The size of the interaction matrix increases as the square of the number of segments. So doubling the memory (currently 128Mb), for example, would not make a big impact on the problem.

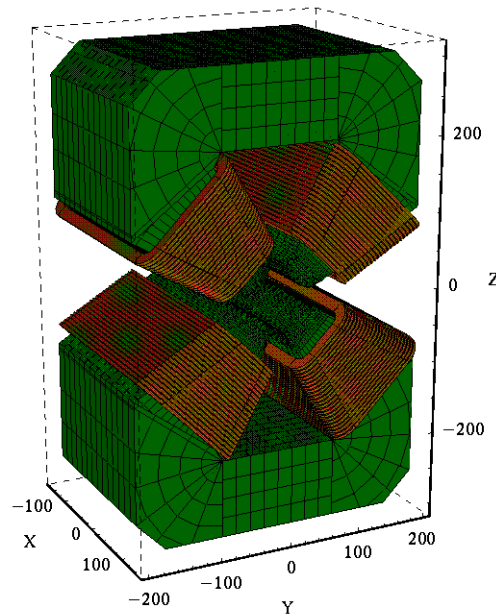


Figure 1. The Q3 Quadrupole as simulated using RADIA.

2. The Simulation

The simulation used the dimensions and pole iron profiles given in Tech. Report 2.1.8G. The simulated quadrupole as rendered by Mathematica is shown in Figure 1. The coordinate system origin is at the geometric centre of the magnet. The x-axis is along the beam direction, the y-axis is horizontal, and the z-axis is vertical.

The simulation included the pole contour to the same accuracy as in the POISSON calculation with the exception that the inside curve where the pole root meets the return iron has been replaced with a straight cut. This is because RADIA cannot define a concave surface. In order to include this curve that section would have to be segmented into many small iron pieces to approximate the curve. This would severely increase the size of the interaction matrix without much benefit. The area in question is far from the quadrupole centre so it should have negligible effect on the field near the centre.

In addition, a chamfer cut on the ends of the pole pieces was included as illustrated in Figure 2. The chamfer angle α was made adjustable to allow optimization of the effective length of the quadrupole.

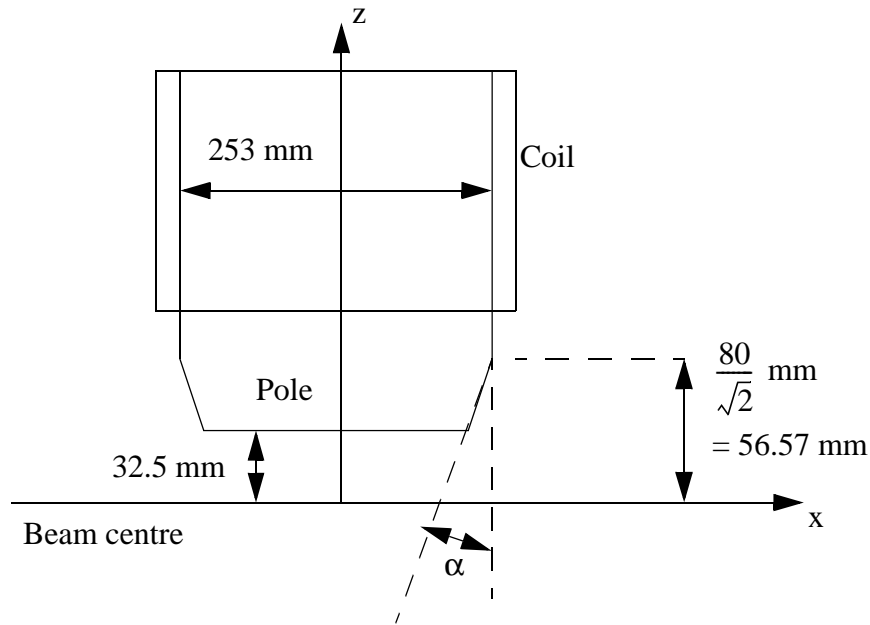


Figure 2. Side view of Q3 pole piece.

The iron used in the simulation was the RADIA pre-programmed material “RadMatSteel42” which is a low carbon steel with $C < 0.13\%$. No attempt was made to adjust for packing factor. This should have minimal effect on the effective length however.

3. Multipole components

In the two dimensions define by the y-z plane it is convenient to express the magnetic field as a complex quantity. At the position defined by

$$\xi = y + iz = re^{i\theta} \quad (1)$$

the complex field is

$$B(\xi) = B_z + iB_y. \quad (2)$$

This may be expanded to

$$B(\xi) = \sum_{n=1}^{\infty} D_n \left(\frac{\xi}{R_{\text{ref}}} \right)^{n-1} \quad (3)$$

where R_{ref} is an arbitrary reference radius, and the complex coefficients are usually written

$$D_n = [C_n e^{-in\alpha_n}]. \quad (4)$$

Usually the complex coefficients, D_n are found by taking a set of ξ 's distributed on a circle of radius R_{ref} in the complex y-z plane, centred on the origin. If multipole coefficients up to order n are required, a set

$$\xi_i = R_{\text{ref}} e^{i\theta_i}, \quad 0 < \theta_i < 360^\circ, \quad i = 1, 2, \dots, n \quad (5)$$

is chosen with the θ_i distributed uniformly on the circle. The fields at this set of positions are then found,

$$B(\xi_i) = B_z(\xi_i) + iB_y(\xi_i). \quad (6)$$

The set of n linear equations

$$B(\xi_i) = \sum_{j=1}^n D_j \left(\frac{\xi_i}{R_{\text{ref}}} \right)^{j-1}, \quad i = 1, 2, \dots, n \quad (7)$$

may be solved for the coefficients D_j . It is usual to define

$$D_j = C_j e^{-ij\alpha_j} = B_j + iA_j, \quad (8)$$

where

$$B_j = \text{“normal” } 2j\text{-pole term}$$

and

$$A_j = \text{“skew” } 2j\text{-pole term.}$$

For example, at the centre of a normal ideal quadrupole, the field at $z = 0$ is \perp to the y-axis. i.e. when ξ_i is real, $B_y = 0$, and therefore the D_j 's must all be real, and therefore $A_j = 0$ and $\alpha_j = 0$.

The above is in the so-called “European” convention, where

$$B_1 = \text{normal dipole term,}$$

$$B_2 = \text{normal quadrupole term,}$$

and

$$B_3 = \text{normal sextapole term, etc.}$$

The magnetic field may also be expanded in a different way (as done by Dallin in 2.1.8G). The magnetic field on the y-axis at $z = 0$ can be written

$$B_z = B_0 + B_0' y + B_0'' y^2 + B_0''' y^3 + B_0'''' y^4 \dots \quad (9)$$

This expansion implicitly assumes the skew terms are zero. If this assumption is correct, these coefficients may be found from

$$B_0 = B_1, B_0' = \frac{B_2}{R_{\text{ref}}}, B_0'' = \frac{B_3}{R_{\text{ref}}^2}, \text{etc.} \quad (10)$$

The magnetic field at the centre of the magnet, i.e. at $x = 0$, should be analysable in the two dimensional way described above since here the field vectors should all be parallel to the $x = 0$ plane. Away from the centre the field is three dimensional and this multipole expansion is no longer valid. However, for most practical purposes one is interested in the *integral* of the field over the length of the magnet. This is because most magnets are short compared to the wavelength of the betatron oscillations in the machine and the details of axial variations in the field are of little consequence. A typical rotating coil will also measure the field integral over the length of the magnet. The above equations may then be used to parameterize the field integral if the magnetic field is everywhere replaced with the field integral.

Note: The expansion parameters $[C_n, \alpha_n]$ or $[B_n, A_n]$ depend on the choice of R_{ref} . The parameters $B_0^{(n)}$ do not. Both sets of coefficients depend on the magnet excitation.

4. Two dimensional field

4.1 Multipole components

We first compare the fields at the centre of the magnet with the two-dimensional POISSON calculation of Dallin (2.1.8G). With the largest number of segments possible with this calculation the results listed in Table 1 were obtained. The POISSON results were calculated for a current of 108.6 A and have been scaled to the current of 118.7 A used in the RADIA calculations. The “estimated error” column is just the change in the results from the RADIA calculation when the segmentation was changed from the next lower degree to the present one. It give some indication of the stability of the answer.

Table 1: RADIA calculation compared with POISSON at x=0

Multipole coefficient	RADIA $R_{\text{ref}} = 10 \text{ mm}$	Estimated error	RADIA $R_{\text{ref}} = 30 \text{ mm}$	Estimated error	POISSON $R_{\text{ref}} = 30 \text{ mm}$
B_0 (G)	0.0158	0.035	23.7	11	-0.773
B_0' (G/cm)	1847	10	1837	2	1925
B_0'' (G/cm ²)	0.0089	0.003	2.54	0.7	0.028
B_0''' (G/cm ³)	-0.115	0.20	-0.00043	0.00015	-0.0019
B_0'''' (G/cm ⁴)	0.00021	0.0007	-0.040	0.0052	0.0013

There are several things to note:

1. Skew terms were always found to be negligible. i.e. A_n was always of the order 10^{-9} T.
2. The quadrupole strength calculated by the 3D code RADIA is lower than that calculated by the 2D code POISSON by about 4%. Since the error on the quadrupole field is small this most likely a real difference. Power supply specifications may need to take this into account. Note however that no attempt was made to account for the packing factor which may further change the power supply requirements.

3. The estimated errors for the multipoles other than the quadrupole term are large. These multipoles do not agree well with the POISSON calculation. This calls into question the confidence one should have in these values calculated by RADIA.
4. Apart from the quadrupole component the other multipole components change dramatically when the reference radius is increased. From the errors in this calculation it is not clear whether this is real or a limitation of the calculation.
5. The above calculation was done with a chamfer angle of 15° on the ends of the pole pieces. The calculation was repeated with a chamfer angle of 30°. This should be far enough from the centre of the quadrupole to have minimal effect on the multipole components calculated at $x = 0$. The quadrupole component changed by only 0.3%, but the other coefficients changed by amount of the order 30%. This is further indication of the limitations of this calculation for calculating multipole components.

4.2 The good field region

The good field region is estimated by plotting

$$\frac{\Delta B}{B_0' y} \quad (11)$$

as a function of y . Here ΔB is defined as

$$\Delta B(y) = B_z(y) - B_0 - B_0' y - B_0'' y^2. \quad (12)$$

The dipole field has been subtracted since it can be compensated by using ring orbit correctors, and the sextapole component has been subtracted since it can be compensated for by adjusting the sextapole magnets in the ring. The coefficients were calculated at the reference radius $R_{\text{ref}} = 10$ mm. The result is plotted with a solid line in Figure 3. Also shown in Figure 3 with a

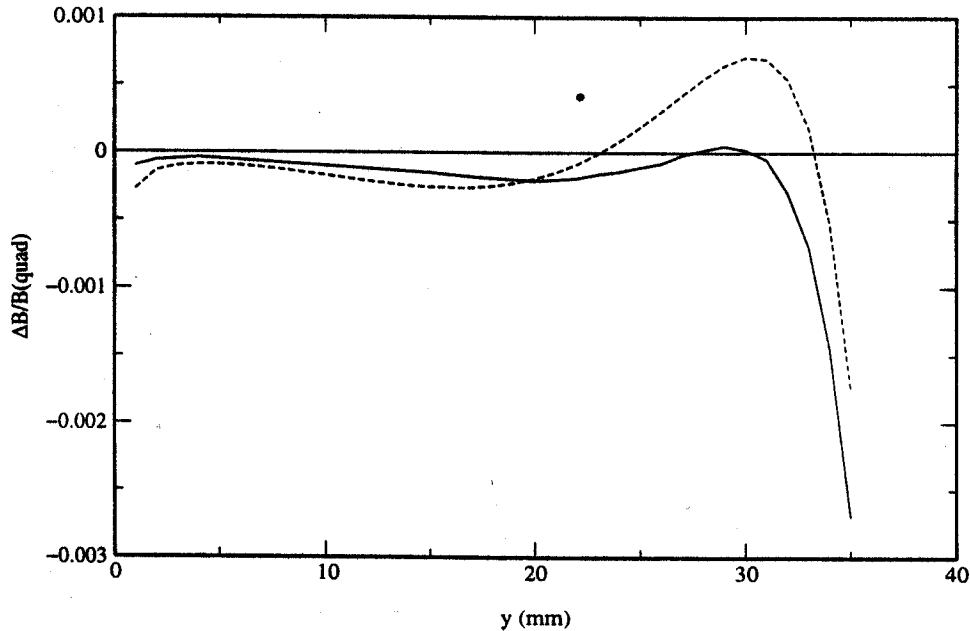


Figure 3. Remnant field at $x = 0$

dashed line is the result from the calculation with the next lower degree of segmentation for the problem. The results show a good field region of less than 0.1% variation in a region of ± 30 mm. However, as discussed in the next section the errors in the computed field values are of this order. So, in light of the errors in the multipole component coefficients discussed in the previous section, this good result may be either simply fortuitous or that the multipole components are indeed small enough so that errors in their calculation are unimportant.

5. Stability of field values

Magnetic fields and effective lengths calculated for the best and next-to-best possible segmentations are compared in Table 2.

Table 2: Comparison of magnetic fields and effective lengths

Value	Best Segmentation	Next-to-best Segmentation
Magnetic field at (0,10 mm,0)	0.18414 T	0.18519 T
Magnetic field at (0,30 mm,0)	0.55248 T	0.55606 T
Field Integral at $y = 10$ mm, $z = 0$	51.498 T.mm	51.803 T.mm
Field Integral at $y = 30$ mm, $z = 0$	154.10 T.mm	155.11 T.mm
Effective Length at $y = 10$ mm, $z = 0$	278.9 mm	278.9 mm
Effective Length at $y = 30$ mm, $z = 0$	279.7 mm	279.7 mm

It can be seen that both the magnet field values and the field integrals are the same to within 0.6%. This suggests (along with other observations not detailed here) that the fields are probably correct to within about 1% at this level of segmentation.

6. Effective Length

The effective length, l_{eff} , is defined to be the distance between the effective (or virtual) field boundaries at either end of the quadrupole. This can be calculated from

$$l_{\text{eff}} B_{z0} = \int_{-\infty}^{\infty} B_z(x) dx \quad (13)$$

where B_{z0} is the uniform field in the centre of the quadrupole and is taken to be the field at $x = 0$.

It can be seen that the effective lengths shown in Table 2 are stable between these two segmentation levels. These calculations were done with a chamfer angle $\alpha = 15^\circ$.

The effect of changing the chamfer angle was investigated using the “next-to-best” segmentation. The results are plotted in figure 4.

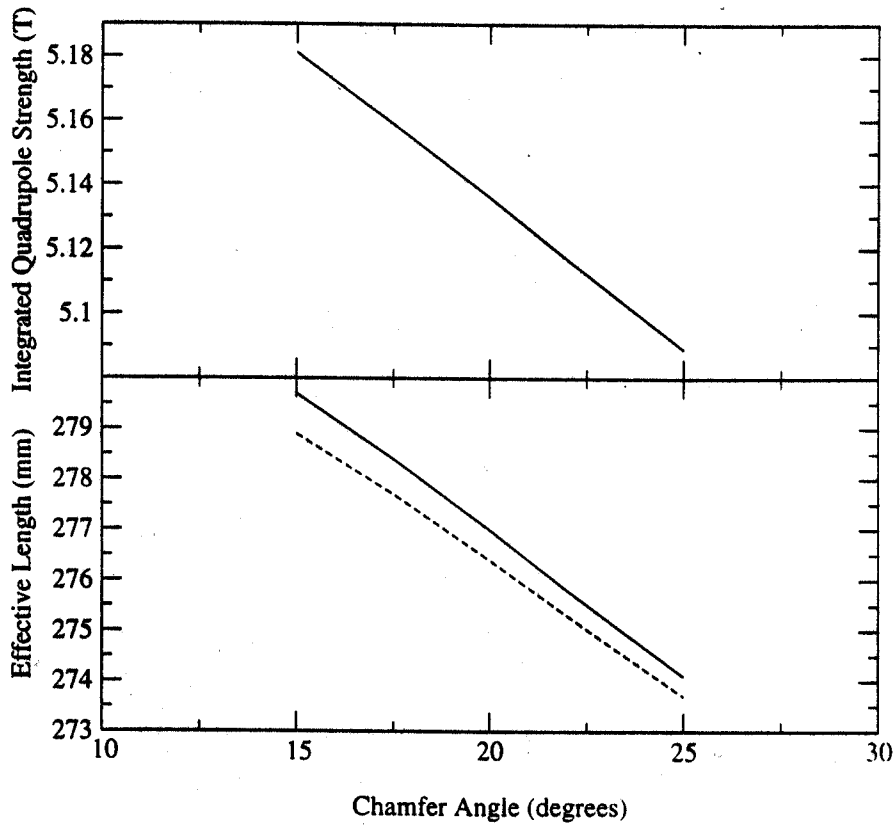


Figure 4. Effect of Chamfer angle

The effective length is shown calculated at $z = 0$ and $y = 10$ mm (solid line) and calculated at $z = 0$ and $y = 30$ mm (dashed line). The required effective length (from Dallin 2.1.8G) is 277 mm. This suggest a chamfer angle of 20° would be appropriate.

Also shown in Figure 4 is the integrated quadrupole strength as a function of chamfer angle. As mentioned in section 3 the multipole components can be extracted for the integrated fields. i.e. we can write (assuming the skew terms are zero)

$$\int_{-\infty}^{\infty} B_z(y) dx = B_1 + B_1' y + B_1'' y^2 + \dots \quad (14)$$

Then

$$l_{\text{eff}}(B_{z0}(y)) = B_1 + B_1' y + B_1'' y^2 + \dots \quad (15)$$

and thus

$$l_{\text{eff}}(B_0 + B_0' y + B_0'' y^2 + \dots) = B_1 + B_1' y + B_1'' y^2 + \dots \quad (16)$$

so the integrated quadrupole strength is

$$B_I' = l_{\text{eff}} B_0' . \quad (17)$$

The Integrated Quadrupole strength shown in Figure 4 is calculated at $R_{\text{ref}} = 10$ mm .

The calculation was repeated with a chamfer angle of zero. The effective length found in this case was 287.9 mm. The phenomenological expression

$$l_{\text{eff}} = l_{\text{iron}} + \alpha R \quad (18)$$

is often used to estimate the effective length for a quadrupole with straight ends. $R = 32.5$ mm is the pole gap radius. This would imply that the parameter $\alpha = 1.07$ in this case.